This article has been accepted for publication in a future issue of this journal, but has not been fully edited. Content may change prior to final publication. Citation information: DOI 10.1109/TIE.2021.3080198, IEEE Transactions on Industrial Electronics

Multi-Port DC-AC Converter with Differential Power Processing DC-DC Converter and Flexible Power Control for Battery ESS Integrated PV Systems

Jiangfeng Wang, *Member, IEEE*, Kai Sun, *Senior Member*, *IEEE*, Cheng Xue, *Student Member, IEEE*, Tingting Liu, and Yunwei Li, *Fellow, IEEE*

***Abstract*—Due to the unpredictable and fluctuating nature of solar photovoltaic (PV), energy storage systems (ESS), such as batteries, are always integrated with PV systems to smooth the power supply. In this paper, a multi-port dc-ac converter (MPC) with differential power processing dc-dc converter (DPPC) is proposed for battery ESS integrated PV systems. The MPC is capable of regulating most of active power among PV, battery and ac grid, and only the differential power (partial power) needs to be handled by the dc-dc converter. Hence, the major merits of higher integration, higher efficiency, and lower cost can be achieved by the proposed configuration. A new cooperative control scheme for the MPC and DPPC is investigated, aiming at realizing flexible active power flow. Besides, a modified space vector pulse-width modulation (SVPWM) is developed for the MPC, taking into the consideration of the voltage variation of both PV and battery. The active power controllability of the MPC and the power rating of the DPPC are quantitatively analyzed. The effectiveness of the proposed configuration, control and modulation schemes is validated by experimental results.**

***Index Terms*—Photovoltaic (PV), energy storage system (ESS), multi-port converter, differential power processing converter, SVPWM strategy.**

I. INTRODUCTION

Due to continually increasing demand for energy and growing concerns over environment, distributed generation (DG) based on renewable energy sources are playing a significant role in modern power systems [1]. Being non-polluting renewable and abundant in most sites, solar photovoltaic (PV) is considered to be one of the most effective alternative energy options [2],[3]. However, the PV output power suffers from intermittence and fluctuation because of high dependence on the natural environment, such as solar irradiance, surrounding temperature and weather, etc. [4]. Therefore, in order to sustain the continuous power supply to the loads, energy storage systems (ESS), such as batteries, are usually integrated with PV systems [5].

Manuscript received December 22, 2020; revised April 4, 2021; accepted April 28, 2021. This work was supported in part by the National Natural Science Foundation of China under Grant 52007098, in part by the Key Project of National Natural Science Foundation of China under Grant 61733010, in part by the China Postdoctoral Science Foundation under Grant 2020M670326, and in part by the Delta Power Electronics Research and Education Development Program under Grant DREM2019005. *(Corresponding author: Kai Sun.)*

Jiangfeng Wang and Kai Sun are with the State Key Lab of Power Systems, Department of Electrical Engineering, Tsinghua University, Beijing 100084, China (e-mail: wangjiangfeng@nuaa.edu.cn, sun-kai@mail.tsinghua.edu.cn).

Cheng Xue and Yunwei Li are with the Department of Electrical and Computer Engineering, University of Alberta, Edmonton, AB, T6G 1H9, Canada (e-mail: cxue1@ualberta.ca, yunwei.li@ualberta.ca).

Tingting Liu is with the Institute of Systems Engineering, China Academy of Engineering Physics, Mianyang 621000, China (e-mail: liutingting@nuaa.edu.cn).

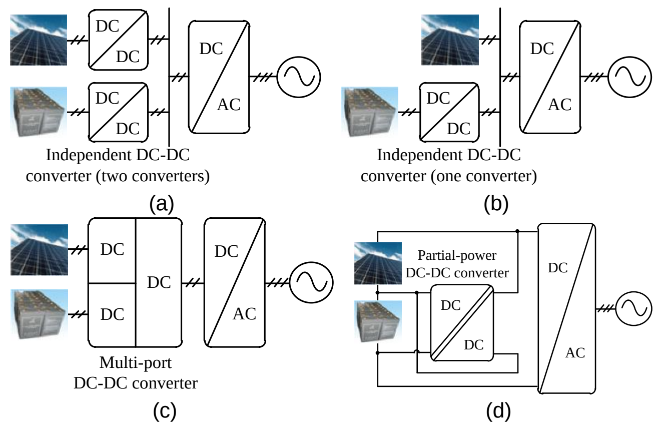

Fig. 1. Dc-coupled battery ESS integrated PV systems: (a) with two independent dc-dc converters [8]-[10], (b) with one independent dc-dc converter [11]-[13], (c) with the multi-port dc-dc converter [14]-[16], (d) with the partial-power dc-dc converter [20].

For an ESS integrated PV system, the power converters are the key to realize flexible active power control among PV, ESS and ac grid. Generally, the architecture of battery ESS integrated PV systems can be classified into two categories: ac-coupled type and dc-coupled type. The most popular ac-coupled integration method is connecting the battery to the common ac bus of PV systems through the individual front-end dc-dc and grid-tied dc-ac converters [6]-[8]. This method features independent flexible power control, but suffers from low efficiency and high cost due to the requirements of too many power converters. Dc-coupled integration methods have gained major interest in recent years since the dc-ac stage is shared by PV and battery [9]-[13]. Two typical dc-coupled integration methods are illustrated in Fig. 1(a) and (b), where PV and battery are connecting to the common dc bus through two [9],[10] or one [11]-[13] independent dc-dc converter, and a centralized dc-ac converter is interfaced with the dc bus and ac grid. The front-end dc-dc converters in this configuration can manage power flow as well as realize voltage match between PV and battery, yet the independent power converters will increase the system cost and size, and decrease the overall efficiency.

Multi-port dc-dc converters, which interface with PV, battery and dc bus simultaneously, are good candidates for the dc-dc stage, as shown in Fig. 1(c). Thanks to the favorable merits of higher power density and higher efficiency compared

This article has been accepted for publication in a future issue of this journal, but has not been fully edited. Content may change prior to final publication. Citation information: DOI 10.1109/TIE.2021.3080198, IEEE Transactions on Industrial Electronics

with independent power converters, the multi-port dc-dc converters have been widely investigated in various dc-dc conversion applications [14]-[16]. Partial-power dc-dc converters shown in Fig. 1(d) are another attractive solution to optimize the dc-dc stage, because only the portion of active power needs to be handled by the dc-dc converter, which, inherently, leads to lower power losses compared to the full-power converter [17]. However, in order to create an independently controlled dc voltage and a direct power flow path, isolated dc-dc topologies should be always employed, resulting in higher circuit complexity and more losses [18], [19]. Another drawback is that this topology is not easy to be modular owing to the complicated circuit connection, resulting in limitations to be extended to high-power applications [20]. The differential power processing converter (DPPC) is another interesting concept, which is used to balance the power of PV elements in PV systems. The basic idea is that the DPPC processes only the difference in power between a PV element and adjacent elements. Since only partial power is processed, the converter power rating can be a fraction of the PV panel's rating, which reduces the converter cost. Till now, the concept of the DPPC is also mainly focused on the dc- dc conversion stage in PV systems [21],[22]. Based on the above, although the multi-port, partial-power and differential power processing dc-dc converters are effective to optimize the dc-dc stage, the back-end dc-ac converter is inevitably needed for ac grid connection, and the multi-stage power conversion still deteriorates the overall efficiency.

To be more integrated and efficient, efforts have been continuously made by researches to further reduce the power conversion stages. An alternative solution is using a cascaded H-bridge based modular bidirectional dc-ac converter to interface with both PV and battery [23]. Nevertheless, this topology faces the major problems of increased H-bridge modules and much complicated control when applied for three-phase systems [24]. Another possible integration method is employing the Z-source/qZ-source bidirectional converter, where PV and battery are connected to the two dc capacitors, respectively [25],[26]. However, several drawbacks, e.g., higher voltage/current stresses, more power losses of switching devices and complicated control, limit the practical applications of these topologies. An interesting solution using only one three-level converter to integrate both PV and battery is investigated in [27], which features simple configuration and high efficiency. Yet, the system cannot work properly with just one battery when PV does not produce any power [27],[28]. To solve this problem, two battery banks and two relays are introduced in this topology, which, in reverse, increases the system complexity and reduces the reliability.

Based on the aforementioned literature review, the multi-port and partial-power conversion techniques have been individually investigated and applied for battery ESS integrated PV systems. Inspired by the state-of-the-art solutions, the primary purpose of our work is aiming at developing a high-integration, high-efficiency and low-cost configuration, by combining both these two techniques. The major contributions of this paper are as follows.

1) The configuration, which consists of a multi-port dc-ac converter (MPC) together with a differential power processing dc-dc converter (DPPC), is proposed for battery ESS integrated PV systems. The MPC is capable of regulating most of active power among PV, battery and ac grid, and only the differential power (partial power) needs to be handled by the DPPC. Hence, the proposed solution features higher efficiency and lower cost. It is worth mentioning that, this work is focused on both the dc-dc and dc-ac stages in battery ESS integrated PV systems, which is different from the traditional DPP configuration focused on only the dc-dc stage in PV systems.

2) Modified control and modulation schemes are proposed for the MPC and DPPC. A new cooperative control scheme, aiming at realizing flexible power flow among PV, battery and ac grid, is studied. A modified space vector pulse-width modulation (SVPWM) strategy is developed for the MPC, with fully considering the voltage variation of both PV and battery.

3) The power controllability of the MPC is quantitatively analyzed. Then the requirements for the power rating of the DPPC can also be derived.

The rest of this paper is organized as follows. In Section II, the basic idea of the MPC with DPPC is introduced, and the related topologies are presented. Modified control and modulation schemes are derived in detail in Section III. Next, the quantitative analysis for the active power controllability of the MPC is provided, and the power rating of the DPPC is obtained in Section IV. Experimental results and discussions are presented in Section V. Finally, key conclusions are drawn in Section VI.

II. Configuration of the MPC with DPPC

A. Derivation of the Configuration

The typical configuration as shown in Fig. 1(b), where PV is directly connected to the dc link, is chosen as the traditional solution for comparison in this paper. Although the voltage of the PV string has certain limitations, this configuration features high efficiency and low cost, and has its own practical applications. The dc-dc converter in Fig. 1(b) is used to regulate the active power and realize voltage match between PV and battery. It is obvious that the dc-dc converter needs to handle all the active power flowing through the battery, and called as full-power dc-dc converter (FPC). Based on this traditional solution, the two-step derivation of the proposed configuration is as follows.

1) In order to reduce power conversion stages and improve the efficiency, the front-end dc-dc converter is reduced, and a new dc port, which is directly connected to the battery, is created in the dc-ac stage. As a result, the configuration of the MPC is derived to interface with PV, battery and ac grid, as shown in Fig. 2(a). The dc-ac converter is called as the MPC because it has three ports (two dc ports and one ac port), which are interfaced with PV, battery and ac grid simultaneously.

2) Considering that the power regulation range of the battery in a stage-stage MPC is always limited by its control and modulation schemes, a DPPC is introduced between two dc ports, to extend the power regulation range, as shown in Fig. 2(b). Assuming that the total active power transferred through the battery is P, and the active power of the battery directly

This article has been accepted for publication in a future issue of this journal, but has not been fully edited. Content may change prior to final publication. Citation information: DOI 10.1109/TIE.2021.3080198, IEEE Transactions on Industrial Electronics

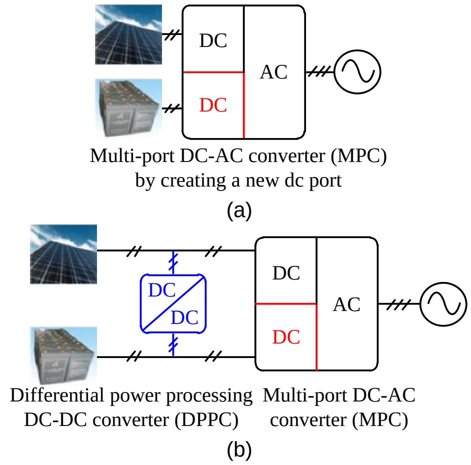

Fig. 2. Derivation of the proposed configuration for battery ESS integrated PV systems: (a) the configuration of the MPC, (b) the configuration of the MPC with DPPC.

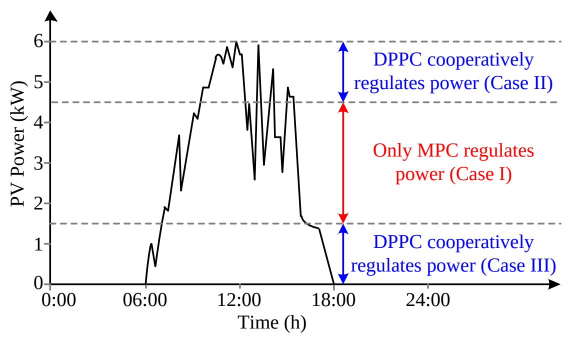

Fig. 3. Typical PV power fluctuation curve within one day.

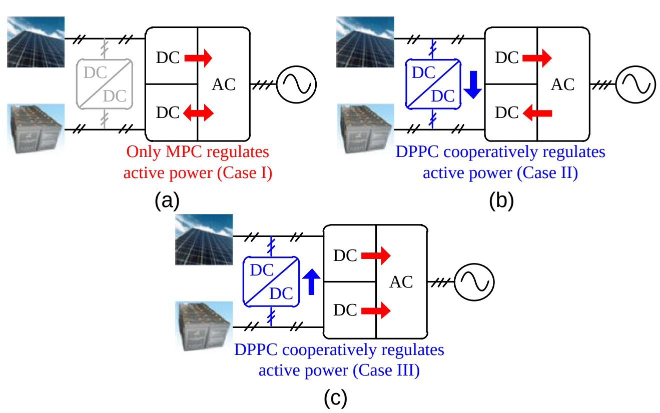

Fig. 4. Basic operation and active power flow of the proposed configuration: (a) Case I, (b) Case II, (c) Case III.

exchanged by the MPC is P_1, the dc-dc converter processes only the difference in power between P and P_1. Hence, the dc-dc converter is denoted as the DPPC.

The core idea of the proposed configuration is that, the MPC is capable of regulating most of active power among PV, battery and ac grid, and only partial active power needs to be processed by the DPPC. A typical PV power fluctuation curve within one day is given in Fig. 3. The basic operation and active power flow of the proposed configuration is shown in Fig. 4. It is seen that, when PV power varies within a certain range, only the MPC operates to realize active power regulation of PV and battery, without using the DPPC, as shown in Fig. 4(a). In this case (Case I), all the active power is transferred within single power conversion stage, featuring high efficiency. When PV power fluctuation exceeds the certain range, the DPPC starts to work and handles the differential power that cannot be regulated by the MPC. Since only partial power is processed by the DPPC, it features low power rating and low cost. In the case that the PV power is very high (Case II), the sufficient PV power will charge the battery through the DPPC, as shown in Fig. 4(b), while in the case that the PV power is very low and even to zero (Case III), partial power of the battery will transfer to the ac grid through the DPPC, as shown in Fig. 4(c).

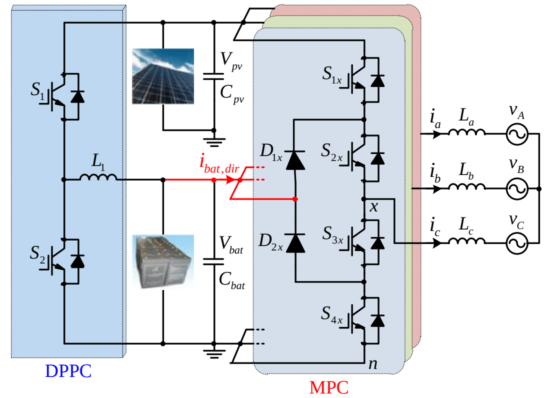

Fig. 5. Topologies of the MPC and DPPC.

B. Topologies

The MPC topology can be derived from the traditional three-level converter, as shown in Fig. 5. It is seen that one of the voltage-dividing capacitors of the traditional three-level converter is separated as a new dc port, and interfaced with the battery, while the original dc link is used as the other dc port, and interfaced with PV. The neutral-point-clamped (NPC) three-level converter is chosen in this paper to derive one MPC topology, and the same method is also suitable to derive other MPCs based on different three-level topologies. It is worth mentioning that, the MPC can also be derived from traditional topologies which have two potential dc ports, such as the Z-source/qZ-source topology and split-source topology. Among these topologies, the three-level topologies are chosen in this paper because they are simpler and more widely-used in practical applications. In Fig. 5, by properly controlling the switches S_{1x}, S_{2x}, S_{3x} and S_{4x} (x=a, b, c), the power flow control among PV, battery and ac grid can be achieved. It is inherent for the MPC that the middle point voltage is not always balanced (i.e., the battery voltage is not always equal to the half of the PV voltage) when the voltages of PV and battery vary. This would lead to the major differences of the control and modulation schemes for the MPC.

As for the DPPC topology, bidirectional dc-dc converters are required due to the bidirectional power flow of batteries. In this paper, a simple buck/boost bidirectional dc-dc converter is employed as an example to illustrate the system operation.

In Fig. 5, the grounds of the PV and battery sources are connected to the same point, which means the proposed configuration is non-isolated. The proposed configuration is also compared with the state-of-the-art non-isolated solutions.

III. Proposed Control and Modulation Schemes

A. Proposed Control Scheme

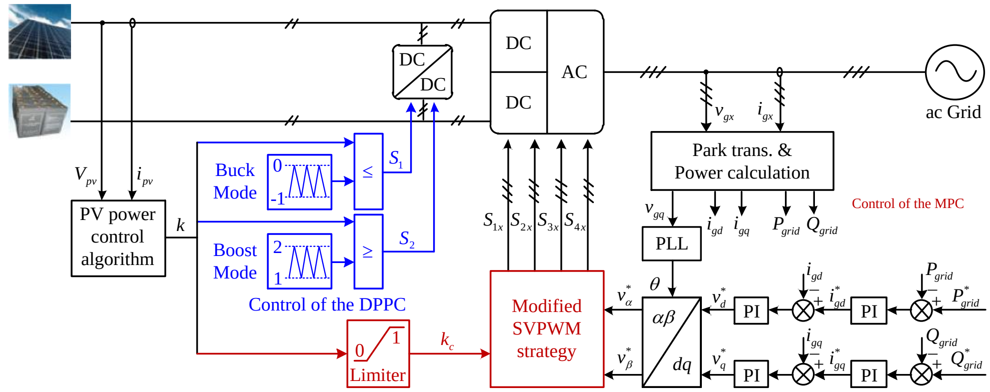

Fig. 6. Block diagram of the proposed power control scheme.

For the proposed configuration, the target is to realize high-efficiency power delivery of PV and battery. To achieve this target, the control logic should be as follows: (1) Within the power control capability of the MPC, it is preferred to use the single-stage MPC to regulate the active power of PV and battery; (2) Only beyond the power control capability of the MPC, the DPPC is introduced to participate in power regulation.

Since the MPC topology is derived from the traditional three-level converter, the idea to realize active power control of the MPC can refer to the voltage balance process of three-level converters. As is known, the voltage balance of three-level converters is always realized by regulating the ratio of positive and negative small vectors in the SVPWM algorithm. Actually, the process to realize voltage balance is physically the process to realize active power regulation of the two capacitors. This drops us a hint that, the power regulation of PV and battery for the MPC can also be achieved by regulating the ratio of positive and negative small vectors in the modulation strategy.

The block diagram of the proposed power control scheme is given in Fig. 6. As shown, the commonly-used P/Q control is employed to regulate the injected ac grid current. On the dc side, the active power of PV can be regulated by MPPT or other PV power control algorithm, like constant power generation method [4]. Since the PV power and the ac-grid power are both controlled, the active power of the battery can be naturally determined. Based on the above algorithm, the key parts to realize the proposed control logic are highlighted in Fig. 6. The parameter k is the output of the PV power control loop, and k_c ($0 \leq k_c \leq 1$) is the control parameter used to regulate the ratio of positive and negative small vectors. The driving signal of the switch S_1 is generated by comparing k with the triangular carrier varying from -1 to 0, and the driving signal of the switch S_2 is generated by comparing k with the triangular carrier varying from 1 to 2, respectively. With different values of k, the system operates in different cases corresponding to Fig. 4.

(1) ***Case I***: When $0 \leq k \leq 1$, $k_c = k$, the switches S_1 and S_2 both turn off. In this case, only the MPC regulates the active power of PV and battery, by regulating the control parameter k_c, and the DPPC is idle.

(2) ***Case II***: when $k<0$, the control parameter k_c is limited to 0. That means, the power control capability of the MPC reaches one of its limit, and it is still not enough to realize the power control of PV and battery. Then the switch S_1 starts to turn on, and the DPPC works as a buck converter.

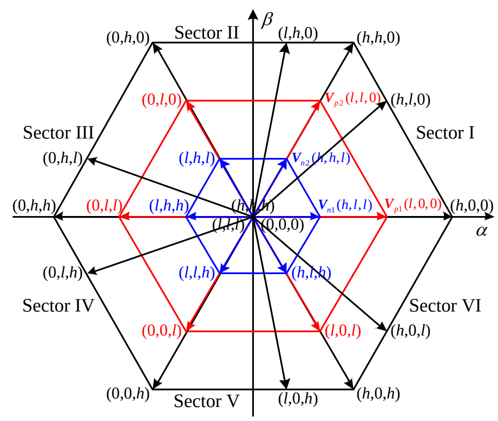

Fig. 7. Voltage space vector diagram of the MPC.

(3) ***Case III***: when $k>1$, the control parameter k_c is limited to 1, indicating that the power control capability of the MPC reaches the other limit. Then the switch S_2 starts to turn on, and the DPPC works as a boost converter.

Based on the above cooperative control scheme for the MPC and DPPC, the target of high-efficiency active power control for the proposed configuration can be achieved. Besides, the SVPWM strategy, and the related power control capability, is another key part, and will be explained in detail in the following sections.

B. Modified SVPWM Strategy

The modified SVPWM strategy is employed for the MPC to realize active power regulation of PV and battery. The switching variable S_x (x=a, b, c), which represents for the midpoint voltage of each switching-leg v_{xn}, is defined according to different switching operation. When S_{1x} and S_{2x} turn on, and S_{3x} and S_{4x} turn off, $v_{xn}=V_{pv}$, and S_x is defined as h. When S_{2x} and S_{3x} turn on, and S_{1x} and S_{4x} turn off, $v_{xn}=V_{bat}$, and S_x is defined as l. When S_{3x} and S_{4x} turn on, and S_{1x} and S_{2x} turn off, v_{xn}=0, and S_x is defined as 0. Combined the switching variable of three phases, the switching states can be defined as (S_a,S_b,S_c). According to the definition, the voltage space vector diagram of the MPC is shown in Fig. 7. Since the voltages of PV and battery are both variable, all the voltage vectors change with the variation of h and l. Particularly, the positive small vectors (marked with the red solid line) and negative small vectors (marked with the blue solid line) are no longer overlapping with each other, except when l=h/2. As a result, the whole space vector diagram is asymmetrically distributed.

This article has been accepted for publication in a future issue of this journal, but has not been fully edited. Content may change prior to final publication. Citation information: DOI 10.1109/TIE.2021.3080198, IEEE Transactions on Industrial Electronics

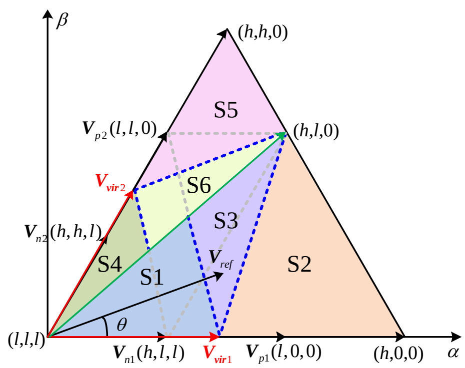

Fig. 8. Division of six sub-sectors.

As mentioned above, the active power control of the MPC can be realized by regulating the ratio of positive and negative small vectors. As seen in Fig. 7, there are two pairs of positive and negative small vectors in each sector. Taking Sector I as an instance, the positive small vector $\boldsymbol{V}_{p1}(l,0,0)$ and the negative small vector $\boldsymbol{V}_{n1}(h,l,l)$ constitutes one pair of small vectors, while $\boldsymbol{V}_{p2}(l,l,0)$ and $\boldsymbol{V}_{n2}(h,h,l)$ forms the other pair of small vectors. Since the positive and negative small vectors are generally not overlapping with each other in Fig. 7, one major challenge of the modified SVPWM scheme for the MPC is the sub-sector division, which is very different from the traditional four or six sub-sector division method used in three-level converters. To deal with this problem, two virtual voltage vectors, i.e., $\boldsymbol{V}_{vir1}$ and $\boldsymbol{V}_{vir2}$, which can be expressed as the following equations, are introduced.

$$\begin{cases} \boldsymbol{V}_{vir1} = k_c \boldsymbol{V}_{p1} + (1-k_c)\boldsymbol{V}_{n1} \\ \boldsymbol{V}_{vir2} = k_c \boldsymbol{V}_{p2} + (1-k_c)\boldsymbol{V}_{n2} \end{cases} \tag{1}$$

where k_c is the control parameter used to regulate the ratio of positive and negative small vectors, as given in Fig. 6.

Based on the virtual voltage vectors, a six sub-sector division scheme is shown in Fig. 8. Since the span of k_c is $0 \le k_c \le 1$, $\boldsymbol{V}_{vir1}$ is located between $\boldsymbol{V}_{p1}$ and $\boldsymbol{V}_{n1}$, and $\boldsymbol{V}_{vir2}$ is located between $\boldsymbol{V}_{p2}$ and $\boldsymbol{V}_{n2}$. The whole Sector I is divided into six sub-sectors, i.e., S1~S6, and these sub-sectors are mainly classified into two groups by the green boundary, which is formed by the zero vector (l,l,l) and the middle vector $(h,l,0)$. Below the blue boundary, it satisfies that

$$\boldsymbol{V}_\beta \le \sqrt{3} v_r \cdot \boldsymbol{V}_\alpha \big/ (2\text{-}v_r) \tag{2}$$

where $v_r = l/h$, and V_α and V_β are coordinates of the reference voltage vector $\boldsymbol{V}_{ref}$ in $\alpha\beta$ frame. In this region, the virtual voltage vector $\boldsymbol{V}_{vir1}$ is used for sub-sector division of S1~S3, which is judged by

$$\text{Sub-sector} = \begin{cases} \text{S1} & \text{if } \boldsymbol{V}_\alpha < (2k_c + 3v_r - 4v_r k_c - 2) \cdot \boldsymbol{V}_\beta \big/ \sqrt{3} v_r \\ & \quad + 2(2v_r k_c + 1 - k_c - v_r) \big/ \sqrt{3} \\ \text{S2} & \text{else if } \boldsymbol{V}_\alpha > (2k_c + v_r - 4v_r k_c) \cdot \boldsymbol{V}_\beta \big/ \sqrt{3} v_r \\ & \quad + 2(2v_r k_c + 1 - k_c - v_r) \big/ \sqrt{3} \\ \text{S3} & \text{otherwise} \end{cases} \tag{3}$$

In the sub-sectors S1~S3, $\boldsymbol{V}_{vir1}$ is always used for the reference vector synthesis and k_c can regulate the active power flow.

Above the blue boundary, it satisfies that

$$\boldsymbol{V}_\beta > \sqrt{3} v_r \cdot \boldsymbol{V}_\alpha \big/ (2\text{-}v_r) \tag{4}$$

In this region, the virtual voltage vector $\boldsymbol{V}_{vir2}$ is used for sub-sector division of S4~S6 and its vector synthesis. The judgment for these sub-sectors is

$$\text{Sub-sector} = \begin{cases} \text{S4} & \text{if } \boldsymbol{V}_\alpha < \dfrac{2v_r k_c + v_r - k_c - 1}{\sqrt{3}(2v_r k_c + 1 - k_c - v_r)} \boldsymbol{V}_\beta + \dfrac{2(1-v_r)}{\sqrt{3}} \\ \text{S5} & \text{else if } \boldsymbol{V}_\beta > \dfrac{\sqrt{3}(1-2v_r)(k_c - 1)}{1 + k_c - 2v_r k_c} \boldsymbol{V}_\alpha \\ & \quad + \dfrac{2(1-v_r)(1 + 2v_r k_c - k_c - v_r)}{1 + k_c - 2v_r k_c} \\ \text{S6} & \text{otherwise} \end{cases} \tag{5}$$

Combined Equs. (2) with (3), and (4) with (5), the sub-sectors S1~S6 can be uniquely determined. After sub-sector division, the reference vector $\boldsymbol{V}_{ref}$ can be synthesized by three nearest vectors, i.e., $\boldsymbol{V}_0$, $\boldsymbol{V}_1$ and $\boldsymbol{V}_2$, in each sub-sector, and the dwell time can be derived by solving the following function.

$$\begin{cases} \boldsymbol{V}_\alpha T_s = \boldsymbol{V}_{0\alpha} T_0 + \boldsymbol{V}_{1\alpha} T_1 + \boldsymbol{V}_{2\alpha} T_2 \\ \boldsymbol{V}_\beta T_s = \boldsymbol{V}_{0\beta} T_0 + \boldsymbol{V}_{1\beta} T_1 + \boldsymbol{V}_{2\beta} T_2 \\ T_s = T_0 + T_1 + T_2 \end{cases} \tag{6}$$

where $\boldsymbol{V}_{i\alpha}$ and $\boldsymbol{V}_{i\beta}$ (i=0,1,2) are coordinates of the voltage vector $\boldsymbol{V}_i$ in $\alpha\beta$ frame, T_i is the action time and T_s is the switching period. After solving the function (6), the virtual voltage vector $\boldsymbol{V}_{vir1}$ can be realized by the real small vectors $\boldsymbol{V}_{p1}$ with the action time $k_c T_i$ and $\boldsymbol{V}_{n1}$ with the action time $(1\text{-}k_c)T_i$, and $\boldsymbol{V}_{vir2}$ can be implemented by $\boldsymbol{V}_{p2}$ and $\boldsymbol{V}_{n2}$ in a similar way. With the above step-by-step process of virtual voltage vector definition, sub-sector division, voltage vector selection, dwell time calculation, and switching sequence arrangement listed in Table I, the modified SVPWM strategy can be finally realized.

TABLE I
SWITCHING SEQUENCE IN EACH SUB-SECTOR

Sub-sector	Switching sequences						
	$0.5k_cT_0$	$0.5T_1$	$0.5T_2$	$(1\text{-}k_c)T_0$	$0.5T_2$	$0.5T_1$	$0.5k_cT_0$
S1	(*l*,0,0)	(*l*,*l*,0)	(*l*,*l*,*l*)	(*h*,*l*,*l*)	(*l*,*l*,*l*)	(*l*,*l*,0)	(*l*,0,0)
S2	(*l*,0,0)	(*h*,0,0)	(*h*,*l*,0)	(*h*,*l*,*l*)	(*h*,*l*,0)	(*h*,0,0)	(*l*,0,0)
S3	(*l*,0,0)	(*l*,*l*,0)	(*h*,*l*,0)	(*h*,*l*,*l*)	(*h*,*l*,0)	(*l*,*l*,0)	(*l*,0,0)
S4	(*l*,*l*,0)	(*l*,*l*,*l*)	(*h*,*l*,*l*)	(*h*,*h*,*l*)	(*h*,*l*,*l*)	(*l*,*l*,*l*)	(*l*,*l*,0)
S5	(*l*,*l*,0)	(*h*,*l*,0)	(*h*,*h*,0)	(*h*,*h*,*l*)	(*h*,*h*,0)	(*h*,*l*,0)	(*l*,*l*,0)
S6	(*l*,*l*,0)	(*h*,*l*,0)	(*h*,*l*,*l*)	(*h*,*h*,*l*)	(*h*,*l*,*l*)	(*h*,*l*,0)	(*l*,*l*,0)

IV. REQUIREMENTS FOR THE POWER RATING OF THE DPPC

In the battery ESS integrated PV system, the battery is used to smooth the PV power, and the power supply of the loads can keep continuous and constant. For the proposed configuration, the active power of the battery P_{bat} is made up of two parts, expressed as

$$P_{bat} = P_{bat,dir} + P_{DPPC} \tag{7}$$

where $P_{bat.dir}$ is the active power directly transferred through the MPC, and P_{DPPC} is the active power processed by the DPPC.

The directly transferred active power $P_{bat.dir}$ is determined by the modified SVPWM scheme of the MPC, which can be derived by

$$P_{bat,dir} = V_{bat} \cdot \int_0^{2\pi} i_{bat,dir}(\theta) d\theta \big/ 2\pi \tag{8}$$

This article has been accepted for publication in a future issue of this journal, but has not been fully edited. Content may change prior to final publication. Citation information: DOI 10.1109/TIE.2021.3080198, IEEE Transactions on Industrial Electronics

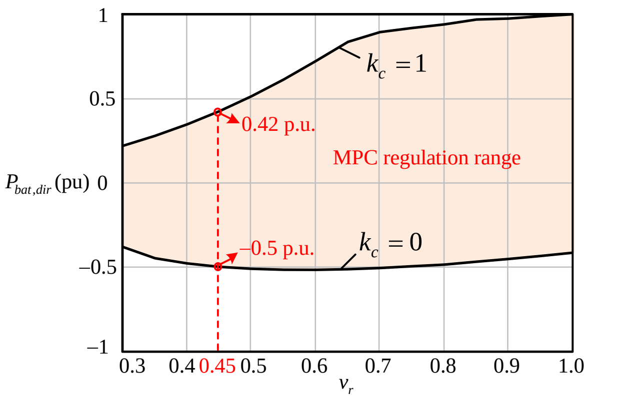

Fig. 9. The normalized directly transferred active power of the battery.

where $i_{bat.dir}(\theta)$ is the average value of the directly transferred battery current during one switching period T_s, and it can be calculated by

$$i_{bat,dir}(\theta) = \sum_{i=0,1,2} \left\{ \sum_{x=a,b,c} [B_{xi} \cdot i_x(\theta)] \right\} \cdot T_i(\theta) \Big/ T_s \tag{9}$$

where B_{xi} satisfies that if $S_x = l$, $B_{xi}=1$, while if $S_x = h$ *or* 0, $B_{xi}=0$, and $i_x(\theta)$ is the phase current. Substituting Equ. (9) into Equ. (8), $P_{bat.dir}$ can be obtained.

On the other hand, the ac-grid active power, i.e., the ac-side load power, can be expressed as

$$P_{ac} = 3V_x I_x \tag{10}$$

where V_x and I_x is the RMS value of the ac-grid phase voltage and current, respectively.

Due to power balance of the whole system, it satisfies that

$$P_{pv} + P_{bat} = P_{ac} \tag{11}$$

where P_{pv} represents the fluctuant PV power. Substituting Equ. (7) into Equ. (11), the power processed by the DPPC, P_{DPPC}, is

$$P_{DPPC} = P_{ac} - P_{pv} - P_{bat,dir} \tag{12}$$

To analyze the requirements for the power rating of the DPPC, the following two assumptions are made: (1) The required ac-side load power P_{ac} is constant, which is defined as P_{ac}(pu)=1.0 p.u., and all the active power is normalized by P_{ac}. (2) The fluctuant PV power varies from 0 to 2.0 p.u. Based on the assumptions, the normalized directly transferred active power of the battery $P_{bat.dir}$(pu), in terms of the voltage ratio v_r ($v_r = l/h = V_{bat}/V_{pv}$) is illustrated in Fig. 9. It can be seen that, the power regulation range of the MPC is surrounded by two boundary lines under the condition that k_c=0 and k_c=1, respectively. Taking a specific case that v_r=0.45 as an example, $P_{bat.dir}$(pu) varies from -0.5 p.u. to 0.42 p.u. with k changing from 0 to 1, and Equ. (12) can be further derived as

$$P_{DPPC}(\text{pu}) = \begin{cases} 0.58\text{ p.u.} - P_{pv}(\text{pu}) & \text{if } 0 \le P_{pv}(\text{pu}) < 0.58\text{ p.u.} \\ 0 & \text{if } 0.58\text{ p.u.} \le P_{pv}(\text{pu}) \le 1.5\text{ p.u.} \\ 1.5\text{ p.u.} - P_{pv}(\text{pu}) & \text{if } 1.5\text{ p.u.} < P_{pv}(\text{pu}) \le 2.0\text{ p.u.} \end{cases} \tag{13}$$

According to Equ. (13), P_{DPPC}(pu)=0 when P_{pv}(pu) varies from 0.58 p.u. to 1.5 p.u. This is because that, within this range, the PV power can be regulated by the battery only using the MPC, via regulating a proper parameter *k*. When P_{pv}(pu) is lower than 0.58 p.u., the MPC operates under one limiting condition that k_c=1, $P_{bat.dir}$(pu)=0.42 p.u., and the DPPC starts to operate in the boost mode. When P_{pv}(pu) is larger than 1.5 p.u., the MPC operates under the other limiting condition that

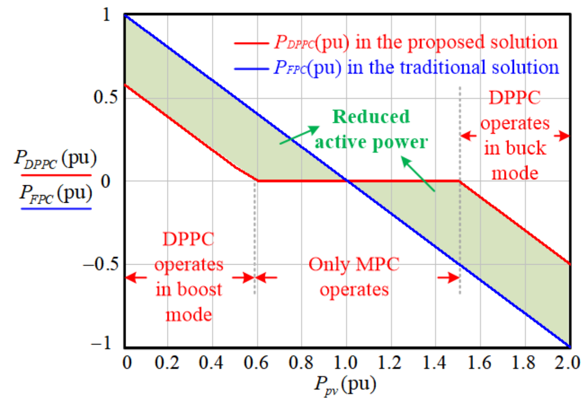

Fig. 10. Active power processed by the DPPC in the proposed solution compared with that processed by the FPC in the traditional solution shown in Fig. 1(b).

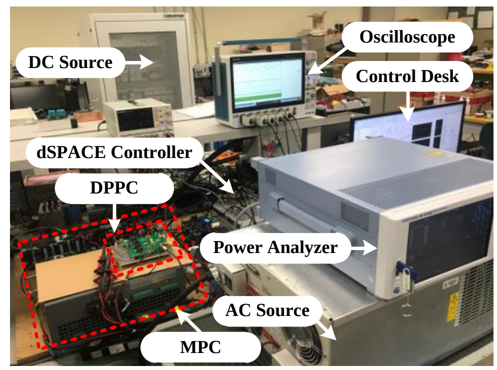

Fig. 11. Experimental prototype.

k_c=0, $P_{bat.dir}$(pu)=-0.5 p.u., and the DPPC starts to operate in the buck mode. The traditional solution shown in Fig. 1(b) is used for comparison, where the normalized power processed by the FPC, P_{FPC}(pu), can be easily derived as

$$P_{FPC}(\text{pu}) = 1.0\text{ p.u.} - P_{pv}(\text{pu}) \tag{14}$$

When P_{pv}(pu) varies from 0 to 2.0 p.u., the curves of P_{DPPC}(pu) and P_{FPC}(pu) are both illustrated in Fig. 10, where it is seen that the active power processed by the DPPC is much lower than that processed by the FPC in the whole PV power variation range. It can be further derived from Equ. (13) and Fig. 10 that, the maximum active power processed by the DPPC is 0.58 p.u. With other values of v_r, the maximum active power processed by the DPPC can be obtained in a similar manner, and the worst case can be used for designing the power rating of the DPPC.

V. Experimental Verification

A. Prototype Description

An experimental platform is constructed and tested to verify the effectiveness of the proposed configuration, control and modulation schemes. The experimental prototype is shown in Fig. 11. The proposed control and modulation schemes are implemented with a dSPACE MicroLabBox DS1202. A programmable ac source from California Instruments is used for emulating the grid, and the rated grid voltage/frequency is 55 V/60 Hz. The rated grid-side active power is 500 W. Two programmable dc sources from REGATRON are used for emulating PV and battery. Taking the lithium iron phosphate (LFP) battery, whose operation voltage varies from 2.5 V to

This article has been accepted for publication in a future issue of this journal, but has not been fully edited. Content may change prior to final publication. Citation information: DOI 10.1109/TIE.2021.3080198, IEEE Transactions on Industrial Electronics

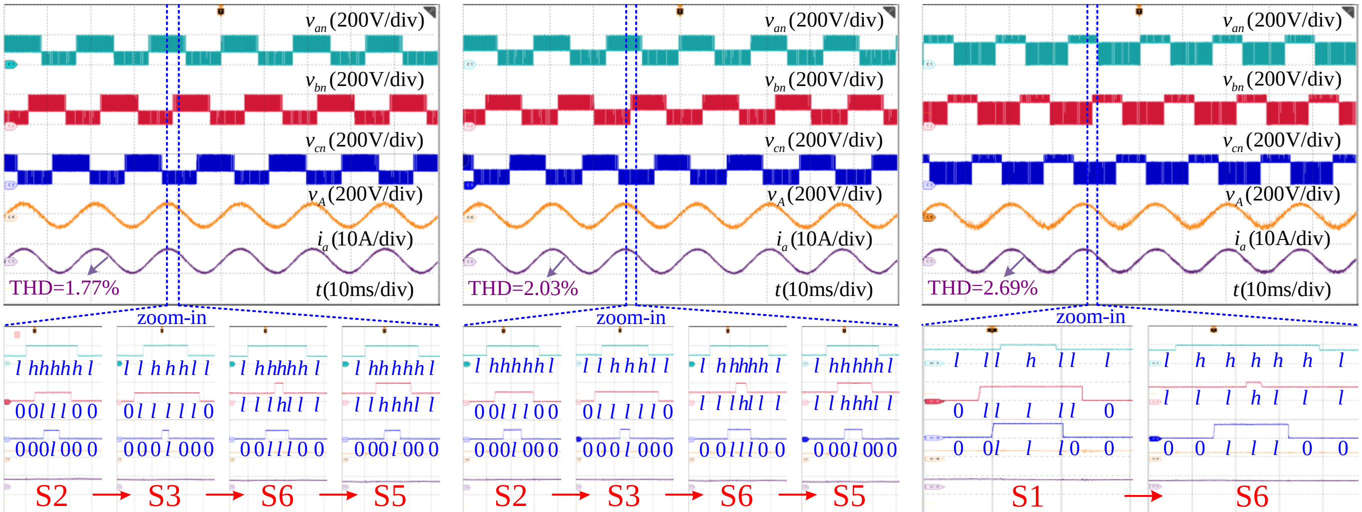

(a) (b) (c)

Fig. 12. Experimental results of the switching sequences: (a) V_{bat}=90 V, (b) V_{bat}=100 V, (c) V_{bat}=150 V.

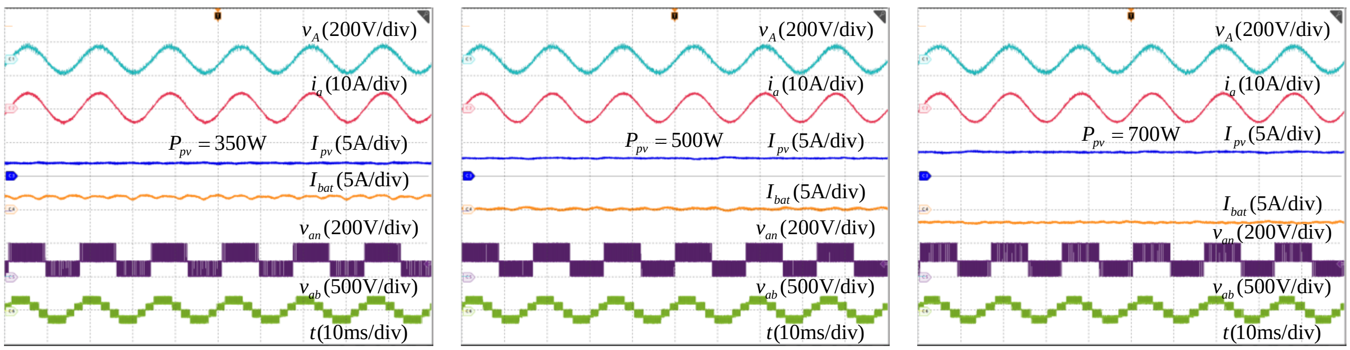

(a) (b) (c)

Fig. 13. Steady-state waveforms when the proposed configuration operates in Case I: (a) P_{pv}=350 W, (b) P_{pv}=500 W, (c) P_{pv}=700 W.

3.65 V [29], as instances, the battery voltage range is 100 V to 146 V with the serial numbers of LFP cells chosen as 40. In this paper, a relatively larger voltage range, i.e., 100-150 V, is chosen for the batteries. The fluctuant PV power varies from 0 to 1 kW, and the PV voltage range is chosen as 180-210 V, which is always larger than the peak value of ac line voltage and the batteries. The MPC is implemented with three insulated gate bipolar transistors (IGBTs) power modules (Infineon F3L75R07W2E3), and the DPPC is implemented with two SiC metal-oxide-semiconductor field-effect transistors (MOSFETs) (ROHM SCT3080KR). The Yokogawa WT5000 Precision Power Analyzer is used for efficiency measurement.

B. Steady-state Operation

To verify the modified SVPWM scheme for the MPC, the experimental tests under the conditions that V_{bat}=90 V, 100 V and 150 V are conducted. The steady-state waveforms of the switching sequence are given in Fig. 12. In the cases that V_{bat}=90 V and 100 V, the reference voltage vector $\boldsymbol{V}_{ref}$ rotates anti-clockwise through S2, S3, S6 and S5, and in the case that V_{bat}=150 V, $\boldsymbol{V}_{ref}$ rotates anti-clockwise through S1 and S6. It is seen that the switching sequences of these sub-sectors fully agree with the theoretical switching sequences listed in Table I. For instance, when $\boldsymbol{V}_{ref}$ rotates through S6, the switching sequences are $(l,l,0)\rightarrow(h,l,0)\rightarrow(h,l,l)\rightarrow(h,h,l)\rightarrow(h,l,l)\rightarrow(h,l,0)\rightarrow(l,l,0)$ as shown in Fig. 12, which is compatible with those in Table I. Besides, it is also seen that the midpoint phase voltages v_{xn} are symmetrical only when the battery voltage V_{bat} is equal to half of the PV voltage V_{pv} (i.e., V_{bat}=100 V), while it is asymmetrically distributed in other cases. The total harmonic distortion (THD) values of the injected grid current under the conditions that V_{bat}=90 V, 100 V and 150 V are 1.77%, 2.03% and 2.69%, respectively, which are close to each other and indicate that the influence of the asymmetrical multi-level characteristics on THD performances is relatively small.

The experimental results in different cases are tested to verify the operation of the proposed configuration. The steady-state waveforms when the proposed configuration operates in Case I are shown in Fig. 13. In this case, only the MPC is used for power control while the DPPC is idle. As seen in Fig. 13(a), the output PV power P_{pv} is 350 W (less than the grid-side power), and the battery is discharged to provide the residual power required by the grid-side power. In Fig. 13(b), when P_{pv} is 500 W (equal to the grid-side power), it supplies active power to the ac grid without charging/discharging the battery. In Fig. 13(c), when P_{pv} increases to 700 W (larger than the grid-side power), part of the PV power is delivered to the ac grid, while the remainder charges the battery. It is obvious from Fig. 13 that, within a certain range of P_{pv}, e.g., 350-700 W, the MPC is capable to realize active power control among PV, battery and ac grid.

The steady-state waveform when the proposed configuration operates in Case II is shown in Fig. 14. It is seen that, when P_{pv} increases up to 1 kW, the switch S_1 of the DPPC turns on while

This article has been accepted for publication in a future issue of this journal, but has not been fully edited. Content may change prior to final publication. Citation information: DOI 10.1109/TIE.2021.3080198, IEEE Transactions on Industrial Electronics

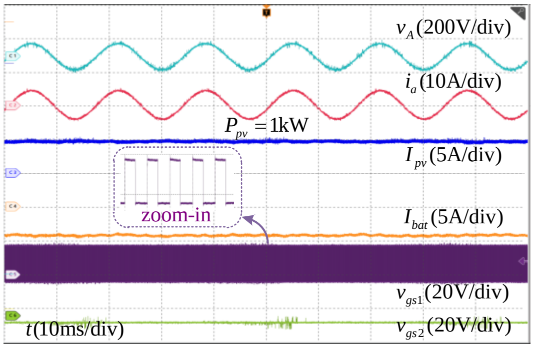

Fig. 14. Steady-state waveform when the proposed configuration operates in Case II (P_{pv}=1 kW).

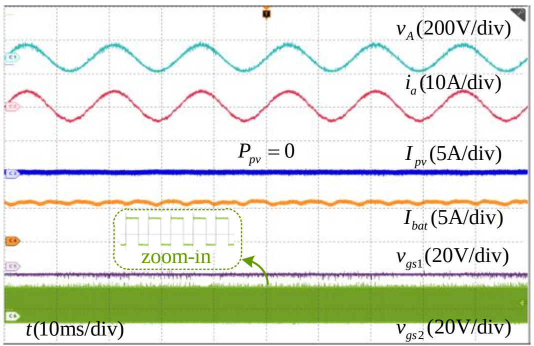

Fig. 15. Steady-state waveform when the proposed configuration operates in Case III (P_{pv}=0).

the switch S_2 remains off, which means the DPPC starts to work in the buck mode. In this case, part of the PV power charges the battery through the MPC, while the other part is processed by the DPPC. When P_{pv} decreases to 0, the steady-state waveform is shown in Fig. 15, where the switch S_1 of the DPPC is off while the switch S_2 turns on and the DPPC operates in the boost mode. In this case, the active power of the battery is delivered to the ac grid in part by the MPC and in part by the DPPC.

In summary, it can be derived from Figs. 13~15 that, the proposed configuration works well in different cases according to the fluctuant PV power, and the experimental results agree with the theoretical analysis pretty well.

C. *Transient Operation*

The transient performance during the load stepping up and down is shown in Fig. 16. As shown, the output PV power keeps constant. When the load steps up, the battery changes from the charging mode to the discharging mode, while when the load steps down, the battery returns to the charging mode.

The dynamic waveform during the large PV power variation (taking the worst case that P_{pv} changes between 0 and 1 kW as an example) is given in Fig. 17. As shown, the load (grid-side power) keeps constant. When the PV power P_{pv} is 1kW, the battery is charged and the DPPC works in the buck mode. As P_{pv} decreases to zero, the battery turns to be discharged and the DPPC changes to work in the boost mode. As seen in Figs. 16 and 17, fast and smooth transient performance is achieved by the proposed configuration.

D. *Comparison with Traditional Solutions*

In order to highlight the advantages of the proposed configuration, the traditional solution shown in Fig. 1(b) is also built and tested for comparison. To make a fair comparison, An

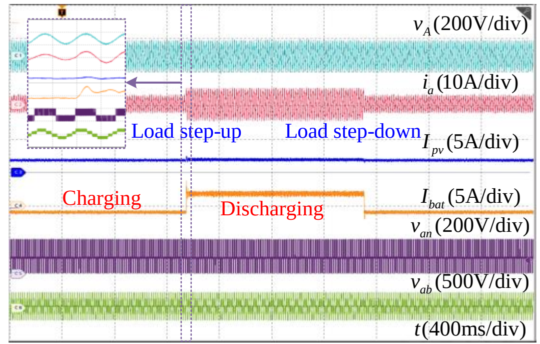

Fig. 16. Dynamic waveform during the load stepping up and down.

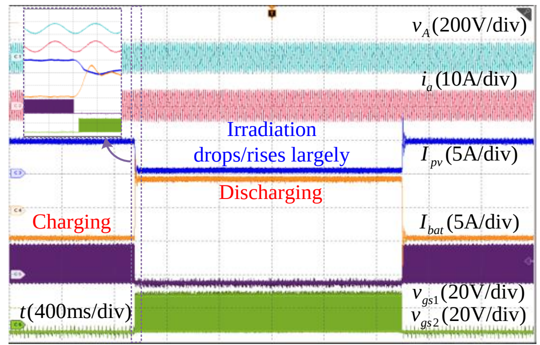

Fig. 17. Dynamic waveform during the large PV power variation.

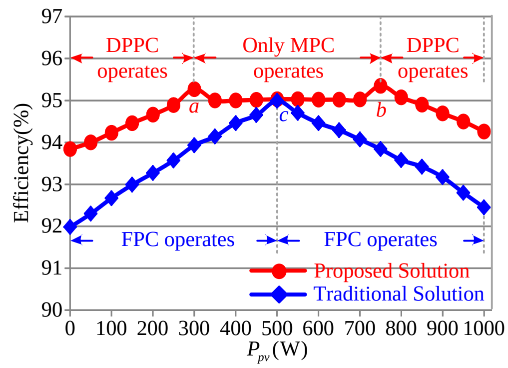

Fig. 18. Efficiency comparison in the whole PV power variation range.

FPC with the same topology as the DPPC, and an NPC three-level dc-ac converter with the same devices and parameters, are used for the traditional solution.

As for the power rating of the dc-dc converter, according to the specification of the prototype and the analysis in Section IV, the maximum active power processed by the DPPC is 0.6 p.u. Therefore, in comparison with the traditional solution, where the maximum power processed by the FPC should be 1.0 p.u., the power rating of the dc-dc converter in the proposed solution can be reduced by 40%.

As for the system efficiency, the efficiency comparison in the whole PV power variation range is shown in Fig. 18. For the proposed solution, the points a and b are near the limiting conditions that k_c=1 and k_c=0, and the efficiency is relatively higher due to the five-segment SVPWM rather than seven-segment SVPWM. In the range between point a and b, only MPC operates and the efficiency is almost constant, while out of this range, the efficiency decreases with the increasing power processed by the DPPC. For the traditional solution, when operating in the point c, the PV power is equal to the grid-side power, and the battery and FPC are idle. Hence, the efficiency in this point is almost the same as the proposed solution. Expect for this point, the efficiency of the traditional solution is lower than that of the proposed solution due to much more power processed by the FPC. As seen, the maximum efficiency improvement of the proposed solution is almost 2%.

E. Discussions for Practical Applications

Based on the theoretical analysis and experimental results, the proposed configuration can interface with two dc ports and one ac port, simultaneously, and realize flexible power control among these ports. Besides, some attractive features, such as much lower power rating of the dc-dc converter between two dc ports, and much higher conversion efficiency, are achieved. It has been verified in this paper that the battery ESS integrated PV systems are good applications. Moreover, the same concept of this paper can also be extended to hybrid energy systems (e.g., the two dc ports interface with the super-capacitor and battery), micro-grids and other practical applications.

VI. Conclusion

A multi-port dc-ac converter (MPC) with differential power processing dc-dc converter (DPPC) is proposed in this paper for battery ESS integrated PV systems. A cooperative control scheme for the MPC and DPPC, aiming at realizing flexible active power control and smoothing the full range of PV power fluctuation, is developed. Moreover, a modified SVPWM scheme is investigated for the MPC, with fully considering the voltage variation of both PV and battery. Based on the proposed control and modulation schemes, the MPC is capable of regulating most of active power among PV, battery and ac grid, and only the differential power (partial power) needs to be processed by the DPPC. The power control capability of the MPC and the requirements for the power rating of the DPPC is analyzed in detail. With the specification of the prototype, the power rating of the dc-dc converter can be reduced by 40%, and the system efficiency improvement can reach up to 2%. Therefore, the proposed configuration features some attractive advantages, e.g., more integrated, more efficient and more cost-effective, and it is a good candidate for practical applications, such as battery ESS integrated PV systems, hybrid energy systems, micro-grids, etc.

References

[1] J. M. Guerrero et al., "Distributed generation: Toward a new energy paradigm," *IEEE Ind. Electron. Mag.*, vol. 4, no. 1, pp. 52–64, Mar. 2010.

[2] X. Zhang, Q. Gao, Y. Hu, H. Zhang and Z. Guo, "Active Power Reserve Photovoltaic Virtual Synchronization Control Technology," *Chin. J. Elect. Eng.*, vol. 6, no. 2, pp. 1–6, 2020.

[3] A. Ibrahim, M.B. Shafik, M. Ding, Mohammad Abu Sarhan, Z. Fang, Ahmed. G. Alareqi, Tariq Al'moqri, Ayman. M. Al-Rassas, "PV Maximum Power-point Tracking Using Modified Particle Swarm Optimization under Partial Shading Conditions," *Chin. J. Elect. Eng.*, vol. 6, no. 4, pp. 106–121, 2020.

[4] A. Sangwongwanich, Y. Yang and F. Blaabjerg, "High-Performance Constant Power Generation in Grid-Connected PV Systems," *IEEE Trans. Power Electron.*, vol. 31, no. 3, pp. 1822-1825, Mar. 2016.

[5] Y. Shan, J. Hu, M. Liu, J. Zhu and J. M. Guerrero, "Model Predictive Voltage and Power Control of Islanded PV-Battery Microgrids With Washout-Filter-Based Power Sharing Strategy," *IEEE Trans. Power Electron.*, vol. 35, no. 2, pp. 1227-1238, Feb. 2020.

[6] H. Mahmood, D. Michaelson and J. Jiang, "Strategies for Independent Deployment and Autonomous Control of PV and Battery Units in Islanded Microgrids," *IEEE J. Emerg. Sel. Topics Power Electron.*, vol. 3, no. 3, pp. 742-755, Sept. 2015.

[7] Y. Karimi, H. Oraee and J. M. Guerrero, "Decentralized Method for Load Sharing and Power Management in a Hybrid Single/Three-Phase-Islanded Microgrid Consisting of Hybrid Source PV/Battery Units," *IEEE Trans. Power Electron.*, vol. 32, no. 8, pp. 6135-6144, Aug. 2017.

[8] O. M. Akeyo, V. Rallabandi, N. Jewell and D. M. Ionel, "The Design and Analysis of Large Solar PV Farm Configurations With DC-Connected Battery Systems," *IEEE Trans. Ind. Appl.*, vol. 56, no. 3, pp. 2903-2912, May/Jun. 2020.

[9] A. Merabet, K. Tawfique Ahmed, H. Ibrahim, R. Beguenane and A. M. Y. M. Ghias, "Energy Management and Control System for Laboratory Scale Microgrid Based Wind-PV-Battery," *IEEE Trans. Sustain. Energy*, vol. 8, no. 1, pp. 145-154, Jan. 2017.

[10] Z. Yi, W. Dong and A. H. Etemadi, "A Unified Control and Power Management Scheme for PV-Battery-Based Hybrid Microgrids for Both Grid-Connected and Islanded Modes," *IEEE Trans. Smart Grid*, vol. 9, no. 6, pp. 5975-5985, Nov. 2018.

[11] V. Narayanan, S. Kewat and B. Singh, "Real-Time Implementation of CLMS Algorithm in 3P4W Solar PV-BES-Based Microgrid System," *IEEE Trans. Ind. Appl.*, vol. 57, no. 1, pp. 795-804, Jan.-Feb. 2021.

[12] S. Devassy and B. Singh, "Performance Analysis of Solar PV Array and Battery Integrated Unified Power Quality Conditioner for Microgrid Systems," *IEEE Trans. Ind. Electron.*, vol. 68, no. 5, pp. 4027-4035, May 2021.

[13] O. M. Akeyo, V. Rallabandi, N. Jewell and D. M. Ionel, "The Design and Analysis of Large Solar PV Farm Configurations With DC-Connected Battery Systems," *IEEE Trans. Ind. Appl.*, vol. 56, no. 3, pp. 2903-2912, May-June 2020.

[14] H. Wu, K. Sun, S. Ding and Y. Xing, "Topology Derivation of Nonisolated Three-Port DC–DC Converters From DIC and DOC," *IEEE Trans. Power Electron.*, vol. 28, no. 7, pp. 3297-3307, Jul. 2013.

[15] Z. Wang, Q. Luo, Y. Wei, D. Mou, X. Lu and P. Sun, "Topology Analysis and Review of Three-Port DC–DC Converters," *IEEE Trans. Power Electron.*, vol. 35, no. 11, pp. 11783-11800, Nov. 2020.

[16] A. K. Bhattacharjee, N. Kutkut and I. Batarseh, "Review of Multiport Converters for Solar and Energy Storage Integration," *IEEE Trans. Power Electron.*, vol. 34, no. 2, pp. 1431-1445, Feb. 2019.

[17] M. Kasper, D. Bortis and J. W. Kolar, "Classification and Comparative Evaluation of PV Panel-Integrated DC–DC Converter Concepts," *IEEE Trans. Power Electron.*, vol. 29, no. 5, pp. 2511-2526, May 2014.

[18] J. R. R. Zientarski, M. L. d. S. Martins, J. R. Pinheiro and H. L. Hey, "Series-Connected Partial-Power Converters Applied to PV Systems: A Design Approach Based on Step-Up/Down Voltage Regulation Range," *IEEE Trans. Power Electron.*, vol. 33, no. 9, pp. 7622-7633, Sept. 2018.

[19] J. W. Zapata, S. Kouro, G. Carrasco, H. Renaudineau and T. A. Meynard, "Analysis of Partial Power DC–DC Converters for Two-Stage Photovoltaic Systems," *IEEE J. Emerg. Sel. Topics Power Electron.*, vol. 7, no. 1, pp. 591-603, Mar. 2019.

[20] N. Kim and B. Parkhideh, "PV-Battery Series Inverter Architecture: A Solar Inverter for Seamless Battery Integration With Partial-Power DC–DC Optimizer," *IEEE Trans. Energy Convers*., vol. 34, no. 1, pp. 478-485, Mar. 2019.

[21] H. Jeong, H. Lee, Y. Liu and K. A. Kim, "Review of Differential Power Processing Converter Techniques for Photovoltaic Applications," *IEEE Trans. Energy Convers.*, vol. 34, no. 1, pp. 351-360, Mar. 2019.

[22] G. Chu, H. Wen, Y. Hu, L. Jiang, Y. Yang and Y. Wang, "Low-Complexity Power Balancing Point-Based Optimization for Photovoltaic Differential Power Processing," *IEEE Trans. Power Electron.*, vol. 35, no. 10, pp. 10306-10322, Oct. 2020.

[23] N. Kim and B. Parkhideh, "Control and Operating Range Analysis of an AC-Stacked PV Inverter Architecture Integrated With a Battery," *IEEE Trans. Power Electron.*, vol. 33, no. 12, pp. 10032-10037, Dec. 2018.

[24] Q. Zhang and K. Sun, "A Flexible Power Control for PV-Battery Hybrid System Using Cascaded H-Bridge Converters," *IEEE J. Emerg. Sel. Topics Power Electron.*, vol. 7, no. 4, pp. 2184-2195, Dec. 2019.

[25] B. Ge et al., "An Energy-Stored Quasi-Z-Source Inverter for Application to Photovoltaic Power System," *IEEE Trans. Ind. Electron.*, vol. 60, no. 10, pp. 4468-4481, Oct. 2013.

[26] S. Hu, Z. Liang and X. He, "Research on the Dynamic Characteristics and Regulation Method of the Energy Stored Quasi-Z-Source Inverter System," *IEEE Trans. Ind. Electron.*, vol. 67, no. 6, pp. 4590-4599, Jun. 2020.

This article has been accepted for publication in a future issue of this journal, but has not been fully edited. Content may change prior to final publication. Citation information: DOI 10.1109/TIE.2021.3080198, IEEE Transactions on Industrial Electronics

[27] H. R. Teymour, D. Sutanto, K. M. Muttaqi, and P. Ciufo, "Solar PV and battery storage integration using a new configuration of a three-level NPC inverter with advanced control strategy," *IEEE Trans. Energy Convers*., vol. 29, no. 2, pp. 354–365, Jun. 2014.

[28] J. Wang, H. Wu, T. Yang, L. Zhang and Y. Xing, "Bidirectional Three-Phase DC–AC Converter With Embedded DC–DC Converter and Carrier-Based PWM Strategy for Wide Voltage Range Applications," *IEEE Trans. Ind. Electron.*, vol. 66, no. 6, pp. 4144-4155, Jun. 2019.

[29] X. Zhang, H. Peng, H. Wang and M. Ouyang, "Hybrid Lithium Iron Phosphate Battery and Lithium Titanate Battery Systems for Electric Buses," *IEEE Trans. Veh. Technol*., vol. 67, no. 2, pp. 956–965, Feb. 2018.

Jiangfeng Wang (S'15-M'19) received the B.S. and Ph. D degrees in electrical engineering and power electronics and power drives from Nanjing University of Aeronautics and Astronautics (NUAA), Nanjing, China, in 2012 and 2018, respectively. Since Mar 2019, he has been a Post-Doctoral Research Fellow with the Department of Electrical Engineering, Tsinghua University, Beijing, China. Since Dec 2019, he has been a Visiting Scholar at Department of Electrical and Computer Engineering, University of Alberta, Edmonton, Canada.

His research interests include high performance converters for hybrid AC/DC microgrids, power quality and distributed power generation system.

Kai Sun (M'12-SM'16) received the B.E., M.E., and Ph.D. degrees in electrical engineering from Tsinghua University, in 2000, 2002, and 2006, respectively. He joined the faculty of Electrical Engineering, Tsinghua University, in 2006, where he is currently a Tenured Associate Professor (Research Professor). From Sep 2009 to Aug 2010, he was a Visiting Scholar at Department of Energy Technology, Aalborg University, Aalborg, Denmark. From Jan to Aug 2017, he was a Visiting Professor at Department of Electrical and Computer Engineering, University of Alberta, Edmonton, Canada. His research interests include power electronics for renewable generation systems, microgrids, and energy internet.

His research interests include high performance converters for hybrid AC/DC microgrids, power quality and distributed power generation system. Dr. Sun serves as an Associate Editor for IEEE Transactions on Power Electronics, IEEE Journal of Emerging and Selected Topics in Power Electronics, and Journal of Power Electronics. Dr. Sun served as the TPC Vice Chair of IEEE ECCE2017 and IEEE ECCE-Asia2017, the Organization Committee Chair of IEEE eGrid2019, and the Publicity Chair of IEEE ECCE2020. He also served as the General Co-Chair of 2018 International Future Energy Challenge (IFEC2018). Dr. Sun serves as PELS Asia Pacific Regional Vice Chair, PELS Beijing Chapter Chair and PELS Electronic Power Grid Systems Technical Committee (TC8) Secretary. He was a recipient of Delta Young Scholar Award in 2013, and Youth Award of China Power Supply Society (CPSS) in 2017, and IEEE Transactions on Power Electronics' Outstanding Reviewers Award in 2019. Dr. Sun is selected as IEEE PELS Distinguished Lecturer in 2021-2022.

Cheng Xue (S'20) received the B. Eng. degree (Yisheng Mao hons.) and M. Sc. degree in electrical engineering from Southwest Jiaotong University, Chengdu, China, in 2015 and 2018, respectively. He is currently working toward the Ph.D. degree in the Department of Electrical and Computer Engineering, University of Alberta, Edmonton, AB, Canada.

His research interests include advanced control of power electronic converters for Microgrid applications and electrical machine drives.

Tingting Liu received the B.S. and M.S. degrees in electrical engineering and power electronics and power drives from Nanjing University of Aeronautics and Astronautics, Nanjing, China, in 2015 and 2018, respectively. She is currently working as an Engineer in the Institute of Systems Engineering, China Academy of Engineering Physics, Mianyang, China.

Her research interests include topology and control of dc–dc and dc–ac converters.

Yunwei Li (S'04-M'05-SM'11-F'20) received the B.Sc. in Engineering degree in electrical engineering from Tianjin University, Tianjin, China, in 2002, and the Ph.D. degree from Nanyang Technological University, Singapore, in 2006.

In 2005, Dr. Li was a Visiting Scholar with Aalborg University, Denmark. From 2006 to 2007, he was a Postdoctoral Research Fellow at Ryerson University, Canada. In 2007, he also worked at Rockwell Automation Canada before he joined University of Alberta, Canada in the same year. Since then, Dr. Li has been with University of Alberta, where he is a Professor now. His research interests include distributed generation, microgrid, renewable energy, high power converters and electric motor drives.

Dr. Li serves as Editor-in-Chief for IEEE Transactions on Power Electronics Letters. Prior to that, he was Associate Editor for IEEE Transactions on Power Electronics, IEEE Transactions on Industrial Electronics, IEEE Transactions on Smart Grid, and IEEE Journal of Emerging and Selected Topics in Power Electronics. Dr. Li served as the general chair of IEEE Energy Conversion Congress of Exposition (ECCE) in 2020. He is the AdCom Member at Large for IEEE Power Electronics Society (PELS) 2021-2023. Dr. Li received the Richard M. Bass Outstanding Young Power Electronics Engineer Award from IEEE PELS in 2013. He is recognized as a Highly Cited Researcher by the Web of Science Group.